CHEMISTRY
A EUROPEAN JOURNAL

DOI: 10.1002/chem.201001876

Catalytic Reaction Mechanism of Mn-Doped Nanoporous Aluminophosphates for the Aerobic Oxidation of Hydrocarbons

Luis Gómez-Hortigüela,*[a] Furio Corà,[a] Gopinathan Sankar,[a] Claudio M. Zicovich-Wilson,[b] and C. Richard A. Catlow[a]

Abstract: In this work we apply state-of-the-art electronic-structure-based computational methods based on hybrid-exchange density functional theory to study the mechanism of the aerobic oxidation of hydrocarbons catalysed by Mn-doped nanoporous aluminophosphates (Mn-AlPOs). We compare our results with available experimental data. We show that the catalytic efficiency of Mn-AlPOs in oxidation reactions is intrinsically linked to 1) the Mn redox activity, in particular between 2+ and 3+ oxidation states, and 2) the coordinative insaturation of tetrahedral Mn embedded in AlPO frameworks, which facilitates the reaction by stabilising oxo-type radicals through the formation of Mn complexes. Our mechanism demonstrates the crucial role of both Mn^{III} and Mn^{II} in the reaction mechanism: Mn^{III} sites undergo an initial reaction cycle that leads to the production of the alkyl hydroperoxide intermediate, which can only be transformed into the oxidative products (alcohol, aldehyde and acid) by Mn^{II}. A preactivation step is required to yield the reduced Mn^{II} sites able to decompose the hydroperoxide intermediates; this step takes place through a transformation of the hydrocarbon into the corresponding peroxo-derivative, stabilised by forming a complex with Mn^{III} and yielding at the same time reduced Mn^{II} sites. Both species enter a subsequent propagation cycle in which Mn^{II} catalyses the dissociation of the hydroperoxide that proceeds until the formation of the oxidative products by two parallel pathways, through alkoxy- or hydroxy-radical-like intermediates, whilst the Mn^{III}–peroxo complex enables further production of the hydroperoxide intermediate.

Keywords: density functional calculations · heterogeneous catalysis · microporous materials · molecular modeling · oxidation · reaction mechanisms

Introduction

Saturated hydrocarbons are among the most abundant yet inert organic compounds, and their selective oxyfunctionalisation at low temperatures is a key goal in contemporary catalytic chemistry. Linear alkanes, such as *n*-hexane, resist attack by boiling nitric acid, concentrated sulfuric acid, chromic acid or potassium permanganate, all of which are oxidants that are no longer environmentally acceptable. Nonetheless, terminal-oxidised alkanes, such as linear alcohols or acids, are of great importance as feedstocks for the chemical and pharmaceutical industries, prompting an intensive search for new ways of selectively oxidising alkanes.

Traditionally, oxidation reactions of alkanes have been catalysed by dissolved salts of redox-active metals. However, current environmental pressure provides a strong incentive to search for new heterogeneous catalytic systems owing to the known problems of homogeneous catalysts associated with handling and reprocessing. Molecular dioxygen is the most environmentally benign and readily available oxidant, but its use still eludes industrial-scale applications. In contrast, the natural biological cycle is supported by atmospheric oxygen, activated in a number of enzymatic reactions; man-made catalysts are still a long way from achieving the activity and selectivity that evolution has given to biosys-

[a] Dr. L. Gómez-Hortigüela, Dr. F. Corà, Prof. G. Sankar, Prof. C. R. A. Catlow
Department of Chemistry, 20 Gordon Street
University College London
WC1H 0AJ London (UK)
Fax: (+44) 2076790493
E-mail: uccalgo@ucl.ac.uk

[b] Dr. C. M. Zicovich-Wilson
Facultad de Ciencias
Universidad Autónoma del Estado de Morelos
Av. Universidad 1001, Col. Chamilpa
Cuernavaca Morelos, 62209 (Mexico)

Supporting information for this article is available on the WWW under http://dx.doi.org/10.1002/chem201001876.

tems. It is in this context that crystalline nanoporous aluminophosphate materials (AlPOs) enter the scenario: AlPOs are zeolite-like materials in which Si ions are replaced by P and Al, forming a three-dimensional oxide network that can adopt many different structures;[1] both ions can be isomorphically replaced by heteroatoms in a controllable manner, giving rise to acid, redox and even bifunctional properties. Of particular importance for oxidation reactions are those materials in which Al ions are replaced by redox-active transition metals, such as Co, Mn and Fe.[2–4] These materials combine the reactivity of redox-active cations with the unique spatial constraints imposed by the molecular dimensions of their porous network.[5–8] Additional important advantages of these catalysts are their high internal surface areas, ease of preparation and high thermal stability.[9] At present, there is extensive experimental research on their performance in different types of oxidations, including the industrially fundamental selective oxidations of *n*-hexane[7,10,11] and cyclohexane,[12–18] the epoxidation of alkenes[19] and the Baeyer–Villiger oxidation of ketones to lactones,[20] all using O_2 as the oxidant.

Whenever chemical transformations are challenging, mechanistic issues come to the fore. Oxidation reactions can be classified into three categories: 1) autoxidation through a free-radical chain reaction; 2) oxidation of the substrate coordinated to the metal ion, followed by reoxidation of the reduced metal and 3) catalytic oxygen transfer.[5,6] The nature of the predominant mechanism depends on the reaction conditions and especially on the nature of the metal and oxidant. One-electron oxidants such as Co, Fe and Mn are known to efficiently catalyse liquid-phase aerobic autoxidation reaction by means of free-radicals, as in category 1).

In free-radical autoxidations, redox-active sites homolytically decompose alkyl hydroperoxide intermediates (ROOH) by Haber–Weiss mechanisms, but do not activate C–H bonds in alkanes through direct reactions with O_2.[21–23] The elementary steps traditionally proposed are summarised in Equations (1)–(7) (in which M = transition metal).[6]

$$RH + O_2 \rightarrow R^{\bullet} + HOO^{\bullet} \quad (1)$$

$$R^{\bullet} + O_2 \rightarrow ROO^{\bullet} \quad (2)$$

$$ROO^{\bullet} + RH \rightarrow R^{\bullet} + ROOH \quad (3)$$

$$ROOH + M^{II} \rightarrow RO^{\bullet} + M^{III}OH \quad (4)$$

$$ROOH + M^{III}OH \rightarrow ROO^{\bullet} + M^{II} + H_2O \quad (5)$$

$$RO^{\bullet} + RH \rightarrow R^{\bullet} + ROH \quad (6)$$

$$ROO^{\bullet} + ROO^{\bullet} \rightarrow ROH + R(H)=O + O_2 \quad (7)$$

The initiation reaction [Eq. (1)] is typically very slow, and gives place to the induction period usually observed in these oxidations; once formed, the alkyl radicals $R^{\bullet}$ rapidly insert oxygen to form peroxy radicals $ROO^{\bullet}$ [Eq. (2)], which can then propagate through hydrogen-transfer reactions to form new alkyl radicals and hydroperoxide (ROOH) [Eq. (3)]. Next the redox sites enter the action: their main role is to promote the homolytic dissociation of the hydroperoxide intermediates to form chain-initiating alkoxy ($RO^{\bullet}$) and alkylperoxy ($ROO^{\bullet}$) radicals [Eqs. (4) and (5)], which undergo new propagation reactions [Eqs. (6) and (3)]. Finally, in the termination step [Eq. (7)], two peroxo-radicals recombine to form the corresponding alcohol and aldehyde in a concerted mechanism.

There is experimental evidence that such a free-radical mechanism applies to the aerobic oxidation of hydrocarbons catalysed by Co- and Mn-containing AlPOs,[7,9,15] as well as for the role of redox active centres in kinetically relevant elementary steps.[8] Nevertheless, no clear knowledge of the mechanism is available. Such knowledge, however, is essential if we are to optimise the regioselectivity of these molecular-sieve catalysts towards the desired terminal oxyfunctionalisation.

The aerobic oxidation of cyclohexane catalysed by MnAPO-5, a Mn-doped aluminophosphate with the AFI framework structure, has been the subject of in depth experimental investigations by Iglesia and co-workers,[15] employing, among others, extensive spectroscopic and isotopic labelling techniques to determine the main reaction intermediates. The reaction scheme proposed in reference [15] was employed as starting point for our computational study; however, in our work we have also examined a selection of alternative mechanistic pathways to those proposed in reference [15], the occurrence of which is difficult to characterise experimentally, but can effectively be discriminated computationally based on the calculated reaction enthalpies and activation energies. The high reactivity of some of the intermediates involved makes them very difficult, if not impossible, to be detected and analysed by experimental techniques. Their molecular structure, especially of those in which the hydrocarbon molecules enter the reaction cycle, will determine the final regioselectivity. In addition, insights concerning the energetics involved—both reaction and activation energies—are needed in order to optimise catalyst performance, yet are difficult to obtain experimentally. This mechanistic and energetic information can be obtained from contemporary computational electronic-structure methods. Comparison of calculated and experimental evidence will serve the purpose of validating both, and will show the powerful atomic-level insight that can now reliably be achieved by combining state-of-the-art complementary methods. As prototypical reaction, we have studied the oxidation of ethane in MnAPO-5 catalysts (see Figure 1 in the Supporting Information). Ethane was chosen as the model hydrocarbon owing to its simple molecular structure and small volume and this allowed us to use expensive periodic DFT techniques rather than cluster models. The choice of ethane means that the issues related to regioselectivity are not studied in the present work; at this stage we are interested only in unravelling the electronic mechanism of the oxidation reaction, for which ethane is entirely appropriate for refining both reaction mechanism and computational parameters.

Even assuming that the energies will be slightly different when using bulkier alkanes and/or secondary or tertiary C atoms, we expect the oxidation mechanism to be largely transferable to other alkane substrates and AlPO frameworks.

Results

The model of the catalytic cycle that we propose consists of a complex mechanism, with preactivation, propagation and regeneration component sybcycles. The first stage of the reaction is a preactivation, summarised in Figure 1. The initial

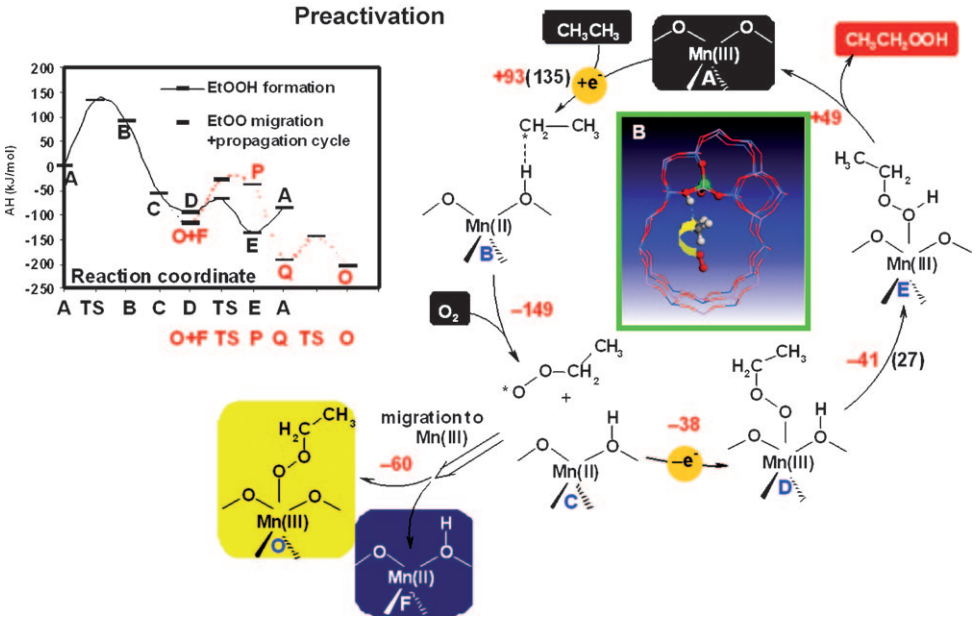

Figure 1. Preactivation mechanism. A black background indicates initial catalyst and reactant molecules, while a red background indicates the hydroperoxide intermediate. Other background colours (yellow, blue) are used to indicate intermediates produced here and necessary to initiate subsequent reaction cycles. Enthalpies (red) and activation energies (black, in brackets), in kJ mol^{-1}, are shown for each elementary step .

reaction conditions involve the presence of the hydrocarbon (RH) (hereafter, the CH_3CH_2 chain will be denoted as R), O_2 and the Mn active site in its oxidised (III) state (**A**). The first elementary step involves the activation of the hydrocarbon through hydrogen transfer to the active site, yielding a Mn^{II} site and an ethyl (R$^{\bullet}$) radical (**B**), which is then rapidly stabilised by the addition of O_2 at the radical's carbon atom from below the CH_2 plane (Figure 1, **B**), giving rise to a free peroxo radical (ROO$^{\bullet}$) (**C**). Due to the orientation of the inserting O_2 molecule, the peroxo radical is located in the middle of the channel. The free ROO$^{\bullet}$ species can reorient and form a complex with Mn^{II} (**D**), resulting in a reoxidation of Mn. Subsequent hydrogen transfer from the framework to the terminal oxygen of the peroxo-ligand yields the hydroperoxide Mn^{III}–ROOH complex (**E**), which can dissociate and release ROOH and free Mn^{III} to undergo subsequent transformations.

This cycle leads to the production and accumulation of ROOH within the catalyst pores, in the presence of Mn^{III}, RH and O_2. ROOH cannot be dissociated through Mn^{III}, since this is a very energetically unfavourable process ($\Delta H = +98$ kJ mol^{-1}); even if this reaction may occur to some extent, it would just yield further ROOH, showing that propagation from ROOH towards the oxidative products (alcohol, aldehyde and acid) can only take place through Mn^{II}. Yet at this point, no reduced Mn^{II} is present in the catalyst as Mn^{II} sites in **C** are subsequently reoxidised in **D**, suggesting that there must be an alternative reaction pathway to induce the net reduction of Mn^{III}. Let us go back to intermediate **C**: the ROO$^{\bullet}$ radical is free in the middle of the channel, near a reduced Mn^{II}. The proximity of ROO$^{\bullet}$ and Mn^{II} suggests their recombination into a Mn^{II}–ROO complex (**D**); however, ROO may also migrate away along the pores of the AFI structure towards another Mn^{III} site, hence leaving behind a Mn^{II} ion in **C**, which would now be available for the dissociation of ROOH (**F**). Indeed, the complex of ROO$^{\bullet}$ with Mn^{III} (**O**) is more favoured than with Mn^{II} (**D**). Interestingly, this process yields not only the required Mn^{II} sites, but also Mn^{III}–ROO complexes (**O**) that, as we shall see below, can also enter the propagation cycle.

Preactivation yields Mn^{II} (**F**), ROOH and Mn^{III}–ROO (**O**), through which the propagation cycle can begin (Figure 2). Two different initiation pathways can take place. ROOH interacts with the Mn^{II} active sites through a hydrogen bond from the framework proton to either the terminal (**G1**) or non-terminal (**G2**) oxygen atoms. The stereochemistry of this hydrogen bond determines the following hydrogen transfer that causes cleavage of the weak O–O bond in ROOH, yielding a molecule of H_2O and an RO$^{\bullet}$ radical (from **G1**) or a molecule of ROH and an OH$^{\bullet}$ radical (from **G2**). The coordinatively insaturated tetrahedral Mn sites stabilise these radicals by forming the corresponding complex (**H** and **L**). These oxo-like complexes activate new hydrocarbon molecules by means of hydrogen transfer from RH to the radical ligands, leading to the production of ROH or H_2O molecules, respectively, and a free R$^{\bullet}$ radical, which is then stabilised by addition of O_2, generating a free ROO$^{\bullet}$ radical (**J** and **L**). Release of ROH or H_2O (**K**) stabilises the ROO$^{\bullet}$ radical by forming a complex with Mn^{III} (**O**), with both mechanisms converging at this step. Indeed, this complex corresponds also to a product

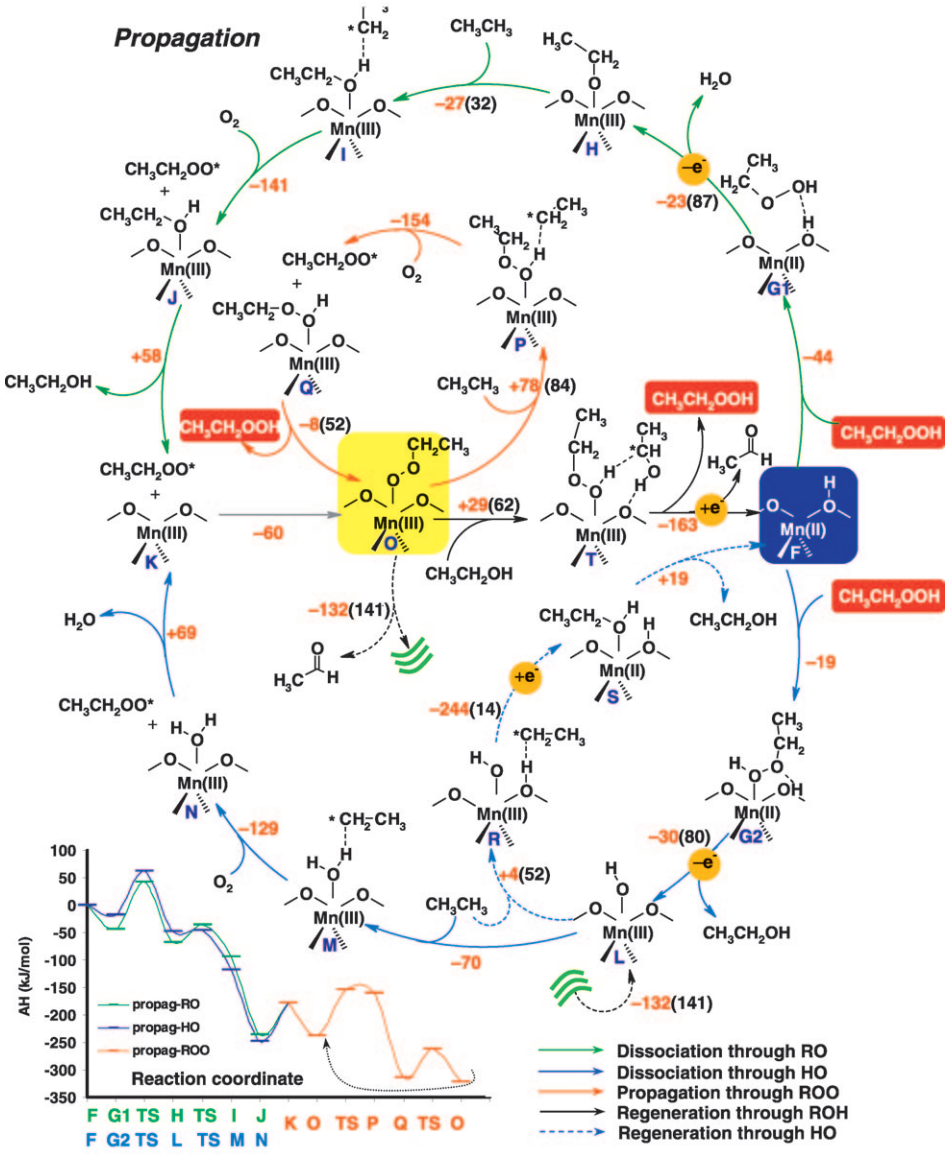

Figure 2. Propagation mechanism. Background colours and energies are represented as in Figure 1.

of the preactivation step (**C**→**F**+**O**, Figure 1), connecting the preactivation and propagation cycles.

The presence of a peroxo-type ligand allows the Mn^{III}–OOR complex (**O**) to activate the hydrocarbon through hydrogen transfer from RH to ROO•, leading to the formation of an Mn^{III}–ROOH complex and an R• radical (**P**) that will then rapidly insert O_2, yielding a free ROO• radical (**Q**). Finally, Mn may exchange ligands, releasing ROOH and binding ROO•, giving rise to ROOH and the Mn^{III}–OOR complex (**O**), thus closing a propagation sub-cycle (red arrows in Figure 2).

Such a sub-cycle produces ROOH, but does not recover the initial Mn^{II} sites. However, ROOH can only be transformed into the final oxidative products by Mn^{II}, as previously discussed. An alternative pathway that allows for the regeneration of the reduced active sites is required in order to close the catalytic cycle.

Regeneration of Mn^{II} may occur by a series of steps that involve the production of the aldehyde (**O**→**L**, dashed black lines) and an alternative RH activation from Mn^{III}–OH (**L**→**R**→**S**→**F**, dashed blue lines). The first step occurs through an intramolecular hydrogen transfer from the C_α of ROO• in (**O**) to the terminal oxygen, prompting the homolytic dissociation of the O–O bond, resulting in an Mn^{III}–OH complex (**L**) and an aldehyde molecule. The complex **L** could then evolve through activation of RH to give H_2O (**M**), as shown previously, but it would finally lead again to Mn^{III}–OOR (**O**), hindering the recovery of Mn^{II}. Activation of RH could take place through an alternative hydrogen transfer not to the OH ligand, but to the framework oxygen of the active site, leading to the $Mn^{III}H$–OH^- intermediate (**R**), which will rapidly evolve by coupling of the two radical-like species (R• and •OH) to yield ROH (**S**), and promoting the reduction of Mn that, after desorption of ROH, would be free to undergo new propagation reactions, thus closing the catalytic cycle. An alternative pathway for the regeneration of Mn^{II} that is more energetically favoured can take place in the presence of ROH. In this mechanism (**O**→**T**→**F**, solid black arrows), hydrogen transfer from the C_α of a previously formed ethanol molecule to the peroxo ROO• ligand takes place, generating an Mn^{III}–ROOH complex and a hydroxyethyl $R_{n-1}HC^{\bullet}(OH)$ radical (**T**). A final hydrogen transfer from the molecular OH group to the framework oxygen provokes the reduction of Mn, yielding the aldehyde and a new molecule of ROOH and also closing the catalytic cycle.

Discussion

Our computational study proposes a complex reaction mechanism that covers the full catalytic cycle of the aerobic oxidation of ethane in MnAPO-5. By replacing the organic radical R or the AlPO polymorph, we expect a similar chemistry to apply to larger hydrocarbons and MnAPO cat-

alysts. The catalytic efficiency of these materials in oxidations is intrinsically linked to 1) the Mn redox activity, in agreement with the relationship between the oxidation rate and the ratio of redox-active Mn sites experimentally observed,[15] and 2) to the coordinatively unsaturated tetrahedral Mn ions embedded in the AlPO frameworks, which facilitate the reaction by stabilising oxo-type radicals (RO•, ROO• and HO•) through the formation of Mn complexes.

The reaction mechanism is based on two main processes: preactivation and propagation. Initially, Mn^{III} sites are preactivated in a series of steps (Figure 1); the first involves a homolytic rupture of the C–H bond, the spin density being transferred to the carbon atom and the active site (Figure 3). This initial step requires a very high activation energy ($\approx 135\ kJ\,mol^{-1}$), which compares very well with the experimentally value for cyclohexane ($155 \pm 10\ kJ\,mol^{-1}$).[15] Such a high activation energy explains the long induction period observed in these oxidations. This initial cycle leads to the production of ROOH, which is indeed the first compound detected experimentally. However, the production of a free ROO• radical (non-bonded to Mn) (**C**) followed by its migration generates Mn^{II} sites (**F**) and Mn^{III}–OOR complexes (**O**)—both active species in the propagation cycle. This preactivation step, in line with that proposed in reference [15], is required just once for each Mn, and so only at the initial stage of the reaction.

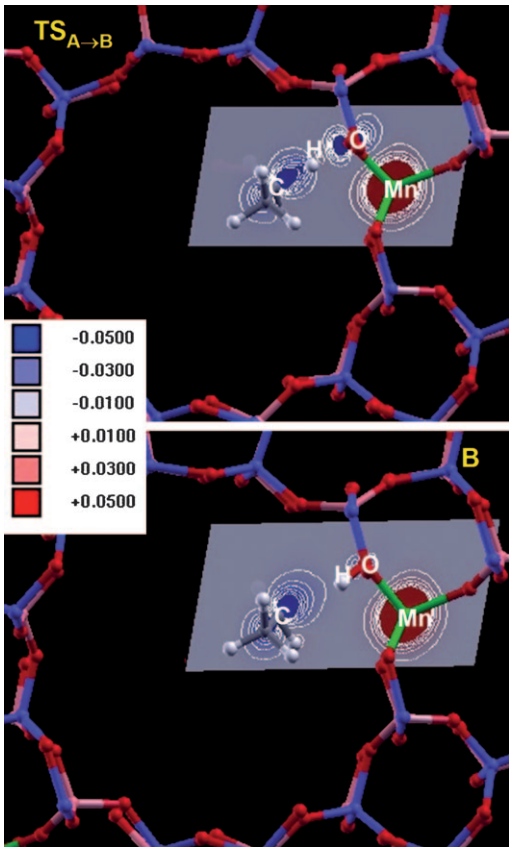

Figure 3. Spin-density maps of the transition state (top) and of Mn^{II}–R• (**B**) (bottom) in preactivation (**A**→**B**). In the transition state, the β-spin density (displayed in blue) from the C–H bond is shared between the carbon atom of RH and the framework oxygen, whilst the α-spin density (red) is strongly-localised on the Mn active site. The formation of Mn^{II}–R• (**B**) brings the complete transfer of the β-spin density well-localised on the radical carbon, whilst the α-spin density is taken by Mn, which is reduced to Mn^{II}. White lines indicate spin isodensity lines.

It is well documented that the addition of radical initiators such as *tert*-butyl hydroperoxide (*t*BuOOH) reduces the induction period,[7,15] which is explained in our model: *t*BuOOH is easily decomposed by Mn^{III} to form Mn^{II} (**F**) and the corresponding peroxo-radical (*t*BuOO•) (Table 1 in the Supporting Information), which could migrate to a nearby Mn^{III} to form the corresponding complex (**F′**) that will then facilitate ROOH production. This mechanism avoids the initial energy-demanding RH direct activation by Mn^{III}, providing an easier Mn preactivation mechanism. Our model also explains the lower reaction rate observed when the catalyst is initially in the reduced form:[15] Mn^{II} is efficient for dissociating ROOH, but cannot itself produce ROOH until it reaches the propagation sub-cycle, for which it requires the presence of ROOH. However, Mn^{II} itself cannot produce the initial ROOH, since it cannot be further reduced to abstract a hydrogen from RH; Mn^{II} would need to be first oxidised to Mn^{III} by O_2 and then carry out the preactivation, decreasing the reaction rate, or it should go through non-catalytic mechanisms.

Once the preactivation has taken place, the two products, Mn^{II} and Mn^{III}–OOR, play separate but complementary roles in the propagation cycle: Mn^{III}–OOR (**O**) is involved in the production of ROOH through the subcycle **O**→**P**→**Q**→**O**. Indeed, this route for ROOH production requires a much lower activation energy ($\approx 84\ kJ\,mol^{-1}$) than through preactivation (**A**→**B**→**C**→**D**→**E**→**A**; $E_a \approx 135\ kJ\,mol^{-1}$), and so represents the main source of ROOH once Mn has been preactivated, as was previously suggested.[15] Mn^{II} is instead engaged in the transformation of ROOH into ROH (and H_2O), finally leading to the Mn^{III}–OOR complex. Two parallel mechanisms can take place, through the formation of RO• or •OH intermediates. The formation of these radicals from ROOH requires high activation energies (≈ 87 and $\approx 80\ kJ\,mol^{-1}$), in good agreement with the experimental value for cyclohexyl–hydroperoxide dissociation ($105 \pm 10\ kJ\,mol^{-1}$).[15] These high activation energies, together with the large atomic rearrangement that this step involves—hydrogen transfer, O–O bond breaking, Mn oxidation and radical complexation—suggest it to be the rate-limiting step in the overall kinetics, as was experimentally observed.[15] The two parallel mechanisms differ in the relative energetics of each step: the initial ROOH dissociation is more favoured through RO•, whilst the RH activation is more favourable through •OH, a consequence of the higher stability of RO• compared to •OH radicals (see Table 1 in the Supporting Information). These processes yield alcohol molecules, which will start to appear in the reaction environment after ROOH.

Once the Mn sites have been preactivated, the RH activation takes place through hydrogen transfer to oxo-radical ligands (alkoxo, peroxo and hydroxo) bonded to Mn^{III} (**H**, **O**

and **L**, respectively). Their efficiency to activate RH is directly related to the stability of the radical, as shown by the OH bond energies (Table 1 in the Supporting Information; O–H bond energies order follows: $H_2O > ROH > ROOH$). The $^{\bullet}OH$ radicals are the least stable, hence explaining their higher efficiency for abstracting hydrogen from RH (**L**→**M**), whilst the opposite is found for ROO$^{\bullet}$ radicals, leading to higher activation energy (**O**→**P**). Additionally, RH may also be activated by Mn^{III}–OH, in which hydrogen is transferred to the framework (**L**→**R**). The pathway whereby these hydrogen transfers take place implies that the forming R$^{\bullet}$ will be located in the channel stabilised by an interaction with the hydrogen atom of the ROH, H_2O or ROOH molecule that is produced (**H**, **L** or **O**, respectively) or to the framework hydrogen (**R**; Figure 4), without R$^{\bullet}$ being directly

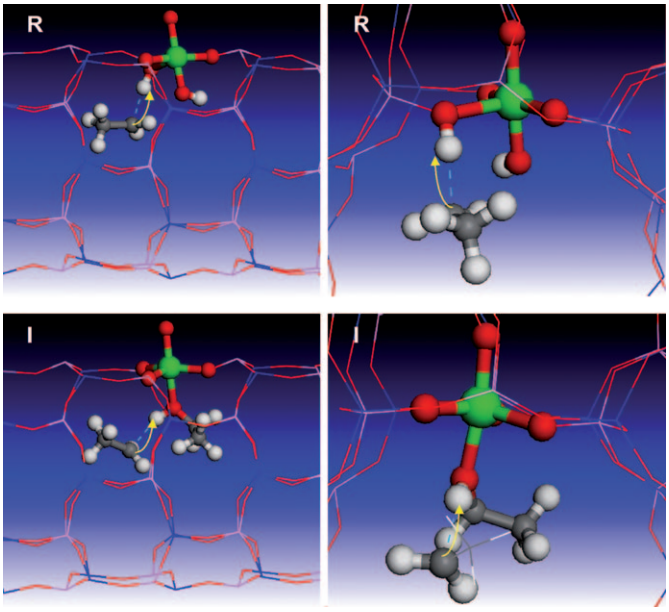

Figure 4. Atomic-level origin of regioselectivity: geometry-optimised structure of Mn^{III}–OH···R$^{\bullet}$ (**R**) (top) and Mn^{III}–ROH···R$^{\bullet}$ intermediates (**I**) (bottom).

bound to the framework (see Figure 5). Modén et al. suggested that the R$^{\bullet}$ radical in steps **I** and **P**, and analogously in **M** in our mechanism (Figure 2), would approach the framework and bind to an oxygen nearest neighbour to Mn. Although the molecular mechanism whereby the hydrogen abstraction from RH occurs leads inevitably to the formation of a free R$^{\bullet}$ radical, it is located in the middle of the channel and stabilised by strong interactions with ROH, ROOH or H_2O (in **I**, **P** and **M** respectively). The R$^{\bullet}$ radical can evolve by binding to the framework, as suggested in reference [15], or through addition of O_2 to form an ROO$^{\bullet}$ radical. We studied computationally the two possibilities for intermediate **I**, but equivalent results are expected for **P** and **M**. The energy diagram for this subset of reactions—bonding of the alkyl radical to the framework oxygen—is shown in Figure 5. Though an activation energy of $\approx 42\ kJ\,mol^{-1}$ is

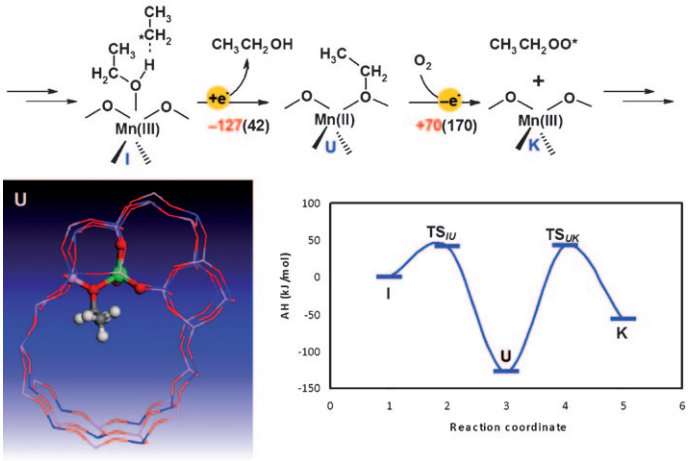

Figure 5. Formation of a complex between CH_3CH_2 radical and Mn through oxygen nearest neighbour to Mn (**U**), and subsequent O_2 attack.

required for the radical to approach the framework, it gives place to a very stable intermediate **U** (Figure 5), the formation process being very exothermic ($\Delta H = -127\ kJ\,mol^{-1}$). The high stability of this complex is due to the net transfer of the unpaired electron from R$^{\bullet}$ to Mn, giving place to the more stable Mn^{II}. In contrast, the competing direct addition of O_2 to the radical needs no activation and is even more exothermic ($-141\ kJ\,mol^{-1}$), suggesting that the oxidation pathway will not take place through the Mn^{II}–R complex (**U**), but through the direct addition of O_2 to the free R$^{\bullet}$ radical. Even if complex **U** is formed, subsequent attack of O_2 to the radical to produce ROO$^{\bullet}$ requires a very high activation energy ($\approx 170\ kJ\,mol^{-1}$), again due to the very high stability of complex **U**, which would lead to the deactivation of the active site, and so ruling out this alternative mechanism.

Once we have identified the full catalytic cycle, its inspection can be used to highlight the individual reaction steps in which we expect regioselectivity to be introduced. Regioselectivity arises in those steps in which RH is activated to generate the alkyl radical R$^{\bullet}$, namely **H**→**I** and **L**→**M** in the ROOH dissociation pathways, **O**→**P** in the propagation subcycle and **R**→**S** in the regeneration. In all cases, the R$^{\bullet}$ radicals are not directly bonded to the framework, but are inside the channel, stabilised by interactions with the transferred hydrogen atom. These proposals need to be explored in future work considering larger hydrocarbon substrates. Regioselectivity is also likely to depend on the special constraints dictated by the AlPO framework structure. Our proposed reaction mechanism may therefore be used to identify the steps and the molecular structure of the intermediates that will dictate the final regioselectivity, which is essential for the design of new Mn-AlPO catalysts.

Incorporation of the O-function always takes place from R$^{\bullet}$ radicals by direct insertion of O_2 in exothermic processes, which provide the main energetic driving force for the oxidation cycle.

A fundamental feature of our mechanism is the complementarity between the two preactivation products, Mn^{II} and

Mn^{III}–OOR: the two species cannot work separately, Mn^{III}–OOR produces ROOH, but cannot convert it to ROH, while Mn^{II} can transform but not produce ROOH. A final reduction of Mn in Mn^{III}–OOR (**O**) is required in order to close the catalytic cycle (regeneration). Regeneration through an intramolecular hydrogen transfer of Mn^{III}–OOR to give aldehyde and Mn^{III}–OH (**O**→**L**), as proposed in reference [15], requires very high activation ($\approx$141 kJ mol^{-1}). In contrast, reduction of Mn through oxidation of ROH to give the aldehyde (**O**→**T**→**F**) is easier ($\Delta H = +29$ kJ mol^{-1}, $E_a \approx 62$ kJ mol^{-1}) due to the lower C–H bond energy of the already oxy-functionalised ROH (Table 1 in the Supporting Information), and hence the latter process will start as soon as ethanol is available in sufficient concentration. This leads to the production of the aldehyde—retarded with respect to ROOH and ROH—and a consequent reduction of the alcohol/aldehyde ratio, in excellent agreement with experimental observations.[15] Indeed, the higher reactivity of the already oxy-functionalised products (lower C–H bond energies; Table 1 in the Supporting Information) indicates that after the first stages of the reaction, these products will undergo secondary oxidation reactions to produce more aldehyde and the corresponding acid in a series of hydrogen-transfer reactions, similar to the previous ones, reducing the alcohol/aldehyde ratio at long reaction times.

Our reaction mechanism compares favourably with the scheme proposed experimentally in references [10,15] and indeed a number of our results do support hypotheses made there. However, the cycle proposed on experimental evidence alone lacks much of the atomic level detail afforded by current computational methods. For instance the cycle in reference [15] contains five intermediates, against 16 from the computational work. Our work, in addition to confirming the experimental analysis in reference [13], reveals a new level of understanding for this complex catalytic cycle. We note in particular that some of the steps quoted in reference [15] are not elementary reaction steps. There are two important steps in which our computational results disagree with reference [15]. First, the alkyl radicals formed at different stages of the reaction are not bonded to the framework. The calculations show that abstraction of hydrogen from the alkane leads to alkyl radicals not directly bonded to the framework.They are instead stabilised by non-bonded interactions with the hydrogen atom transferred; addition of O_2 to these alkyl radicals does occur inside the zeolitic micropores, but is not assisted by the framework. These differences occur in kinetically fast steps, and therefore do not affect the analysis performed in reference [15], but for the same reason they cannot be discriminated experimentally because the experimental techniques available are insensitive to these reaction steps. They can, however, be discriminated by computational studies, and this is an important benefit, since regio- and stereoselectivity, if any, are associated with the stereochemistry of such abstraction/addition processes and differ depending on whether the step occurs in the constrained environment of the alkyl radical coordinated to the framework (as suggested in reference [15]), or relatively unconstrained in the main zeolitic channels (as in our work). The second difference between our cycle and that of reference [15] consists in the regeneration (or termination) step. The mechanism proposed in reference [15] is very unfavourable (we calculated its energy, and found an activation barrier of 141 kJ mol^{-1}), which led us to investigate alternative pathways and propose the **O**→**T**→**F** mechanism that is not mentioned in reference [15]. This mechanism involves the oxidation of a previously formed ethanol molecule to the aldehyde (**O**→**T**), and requires much lower activation energy of 62 kJ mol^{-1}.

In summary, the fact that the main lines of our computationally derived catalytic cycle agree with reference [15] evidences the excellent performance of our computational methodology, against one of the few reactions for which such comparison can be made. This is a necessary step to give confidence on the performance of current electronic structure methods when properly mastered. We believe that our work shows that accurate electronic structure methods are now available, suitable to study even complex heterogeneous catalytic reactions. In this respect, we believe that our work is relevant not only to complement experimental data on the particular reaction we have chosen, but also to show how an entirely new field of computational studies is now ripe.

Conclusion

We have succesfully applied state of the art electronic structure techniques in order to unravel the complex catalytic reaction mechanism of the aerobic oxidation of hydrocarbons catalysed by Mn-doped nanoporous aluminophosphates. Our results show that the catalytic efficiency of Mn-AlPOs in oxidation reactions is based on the Mn redox activity and on the coordinative insaturation of tetrahedral Mn embedded in AlPO frameworks.

An initial preactivation step is required to yield reduced Mn^{II} sites, which are then able to decompose the hydroperoxide intermediates: This preactivation involves a transformation of the hydrocarbon molecules into the corresponding peroxo-derivative, which are then stabilised by forming a complex with Mn^{III} and yielding at the same time reduced Mn^{II} sites. Both species enter a subsequent propagation cycle in which a dual mechanism that requires the presence of Mn in the two different oxidation states is involved, stating the crucial role of the Mn^{III}/Mn^{II} couple: Mn^{III}–OOR is engaged in the production of ROOH, whilst Mn^{II} transforms this ROOH into the final oxidative products through two alternative pathways, through alkoxy- or hydroxy-radical-like intermediates.

Our mechanism is able to rationalise and complement all the experimental observations available in the literature, evidencing the power of electronic-structure-based computational methods in order to study complex catalytic reaction mechanisms.

Computational Methods

In our study we considered the AFI structure (Figure 1 in the Supporting Information) as representative of the class of nanoporous AlPO catalysts: the AFI framework is composed of one-dimensional non-interconnected channels in which all tetrahedral sites are symmetry equivalent and it is one of the most widely used experimentally. The Mn-doped AFI framework was described with periodic boundary conditions, using one crystallographic unit cell (72 atoms) with no symmetry; the AFI unit cell dimensions were large enough to prevent a strong interaction between the reactants in consecutive image cells. One Mn ion (replacing one Al) per AFI unit cell was inserted in a tetrahedral position. This doping level ensured no interaction between image Mn sites. Calculations showed the high-spin state to be the most stable electronic configuration both for Mn^{II} and Mn^{III}, as expected owing to the low crystal field splitting caused by the tetrahedral coordination of the transition metal ions.

We performed density functional theory calculations, as implemented in the program CRYSTAL,[24] using the hybrid functional B3LYP. The excellent comparison between the predicted structure of the active sites in Fe-[25] and Mn-AlPOs[3] using this computational methodology and that obtained by X-ray absorption spectroscopy showed the reliable performance of the computational settings chosen. In order to find the actual reaction pathway and reliably locate all stable intermediates and activation energies, the reactant molecules were approached in discrete steps (usually of 0.1 Å) along the reaction coordinate of each elementary reaction step. At each step, we performed constrained geometry optimisations, keeping the selected reaction coordinate frozen and allowing all the rest of coordinates to relax; this methodology allowed us to obtain the energy diagram for each elementary step along the reaction coordinate, from which we estimated activation energies (calculated as the highest energy value identified along the reaction coordinate). To find the enthalpies for each elementary reaction, full-geometry optimisation calculations of both the reactants and products were performed.

Selected transition state configurations were confirmed by calculating the second-derivative matrix over the whole periodic unit cell.[26] Such Hessian-based techniques are not yet usual in the context of periodic calculations, but were required here to overcome the difficulties associated with the mechanistic complexity of the processes examined, which are not suitable for simpler methods based on nudged elastic bands (NEB) or metadynamics, which rely on the knowledge a priori of the reaction coordinate, nor for adiabatic molecular dynamics simulations due to the high activation barriers.

Acknowledgements

L.G.H. acknowledges funding from EPSRC (grant EP/D504872). F.C. is supported by an RCUK Fellowship. We are grateful to Sir John Meurig Thomas for helpful discussions. The authors acknowledge the use of the UCL Legion High-Performance Computing Facility, and associated support services, in the completion of this work.

[1] http://www.iza-structure.org/databases/.

[2] J. M. Thomas, *Angew. Chem.* **1999**, *111*, 3800–3843; *Angew. Chem. Int. Ed.* **1999**, *38*, 3588–3628.

[3] I. Saadoune, F. Corà, M. Alfredsson, C. R. A Catlow, *J. Phys. Chem. B* **2003**, *107*, 3012–3018.

[4] F. Corà, G. Sankar, C. R. A. Catlow, J. M. Thomas, *Chem. Commun.* **2002**, 734–735.

[5] I. W. C. E. Arends, R. A. Sheldon, M. Wallau, U. Schuchardt, *Angew. Chem.* **1997**, *109*, 1190–1211; *Angew. Chem. Int. Ed. Engl.* **1997**, *36*, 1144–1163.

[6] M. Hartmann, S. Ernst, *Angew. Chem.* **2000**, *112*, 916–918; *Angew. Chem. Int. Ed.* **2000**, *39*, 888–890.

[7] J. M. Thomas, R. Raja, G. Sankar, R. Bell, *Nature* **1999**, *398*, 227–230.

[8] B. Modén, L. Oliviero, J. Dakka, J. G. Santiesteban, E. Iglesia, *J. Phys. Chem. B* **2004**, *108*, 5552–5563.

[9] J. M. Thomas, R. Raja, G. Sankar, R. Bell. *Acc. Chem. Res.* **2001**, *34*, 191–200.

[10] B. Modén, B-Z. Zhan, J. Dakka, J. G. Santiesteban, E. Iglesia, *J. Phys. Chem. C* **2007**, *111*, 1402–1411.

[11] R. Raja, G. Sankar, J. M. Thomas, *Angew. Chem.* **2000**, *112*, 2403–2406; *Angew. Chem. Int. Ed.* **2000**, *39*, 2313–2316.

[12] D. L. Vanoppen, D. E. De Vos, M. J. Genet, P. G. Rouxhet, P. A. Jacobs, *Angew. Chem.* **1995**, *107*, 637–639; *Angew. Chem. Int. Ed. Engl.* **1995**, *34*, 560–563.

[13] F. J. Luna, S. E. Ukawa, M. Wallau, U. Schuchardt, *J. Mol. Catal. A: Chem.* **1997**, *117*, 405–411.

[14] R. Raja, G. Sankar, J. M. Thomas, *J. Am. Chem. Soc.* **1999**, *121*, 11926–11927.

[15] B. Modén, B-Z. Zhan, J. Dakka, J. G. Santiesteban, E. Iglesia, *J. Catal.* **2006**, *239*, 390–401.

[16] P. Concepción, A. Corma, J. M. López-Nieto, J. Pérez-Pariente, *Appl. Catal. A: Gen.* **1996**, *143*, 17–28.

[17] L. Zhou, J. Xu, C. Chen, F. Wang, X. Li, *J. Porous Mater.* **2008**, *15*, 7–12.

[18] M. Dugal, G. Sankar, R. Raja, J. M. Thomas, *Angew. Chem.* **2000**, *112*, 2399–2402; *Angew. Chem. Int. Ed.* **2000**, *39*, 2310–2313.

[19] R. Raja, G. Sankar, J. M. Thomas, *Chem. Commun.* **1999**, 829–830.

[20] R. Raja, J. M. Thomas, G. Sankar, *Chem. Commun.* **1999**, 525–526.

[21] R. A. Sheldon, J. K. Kochi, *Metal-Catalysed Oxidations of Organic Compounds*, Academic Press, New York, **1981**.

[22] C. L. Hill, *Activation and Functionalisation of Alkanes*, Wiley, New York, **1989**.

[23] F. J. Black, *J. Am. Chem. Soc.* **1978**, *100*, 527–535.

[24] CRYSTAL06, R. Dovesi, V. R. Saunders, C. Roetti, R. Orlando, C. M. Zicovich-Wilson, F. Pascale, B. Civalleri, K. Doll, N. M. Harrison, I. J. Bush, Ph. D'Arco, M. Llunell, University of Torino, Torino, **2006**.

[25] C. Zenonos, G. Sankar, F. Corà, D. W. Lewis, Q. A. Pankhurst, C. R. A. Catlow, J. M. Thomas, *Phys. Chem. Chem. Phys.* **2002**, *4*, 5421–5429.

[26] J. Simmons, J. Nichols, *Int. J. Quantum Chem. Symp.* **1990**, *38* (S24), 263–276.

Received: July 2, 2010
Published online: November 24, 2010

